Electronic Supplementary Material (ESI) for Energy & Environmental Science
This journal is © The Royal Society of Chemistry 2013

Supporting Information

A Series of Metal-Organic Frameworks with high Methane Uptake and An Empirical Equation for Predicting Methane Storage Capacity

Yabing He,[a] Wei Zhou,*[b,c] Taner Yildirim,[b,d] and Banglin Chen*[e]

[a] *College of Chemistry and Life Sciences, Zhejiang Normal University, Jinhua 321004, China*

[b] *NIST Center for Neutron Research, Gaithersburg, Maryland 20899-6102, USA.*

[c] *Department of Materials Science and Engineering, University of Maryland, College Park, Maryland 20742, USA. E-mail: wzhou@nist.gov*

[d] *Department of Materials Science and Engineering, University of Pennsylvania, Philadelphia, Pennsylvania 19104-6272, USA.*

[e] *Department of Chemistry, University of Texas at San Antonio, One UTSA Circle, San Antonio, Texas 78249-0698, USA. Fax: (+1)-210-458-7428; E-mail: Banglin.Chen@utsa.edu*

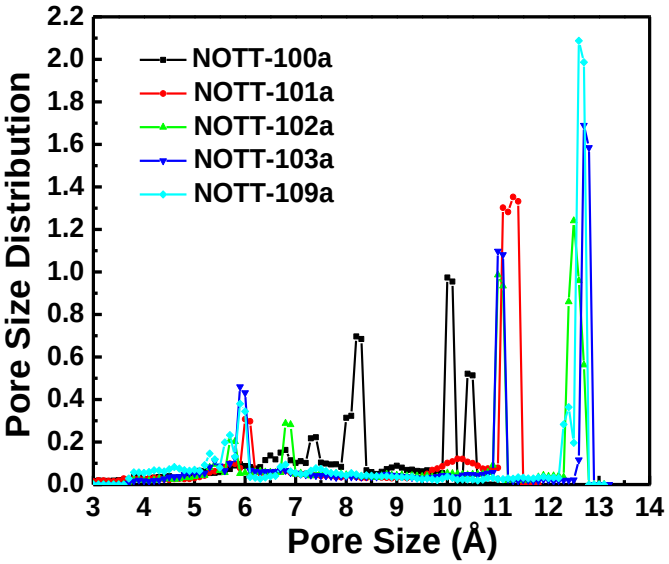

Figure S1. Pore size distributions (PSDs) of **NOTT-100a**, **NOTT-101a**, **NOTT-102a**, **NOTT-103a**, and **NOTT-109a**. PSDs were calculated using the well-known method by Gubbins et al.[29] The van der Waals diameters of the framework atoms were adopted from the Cambridge Crystallographic Centre.

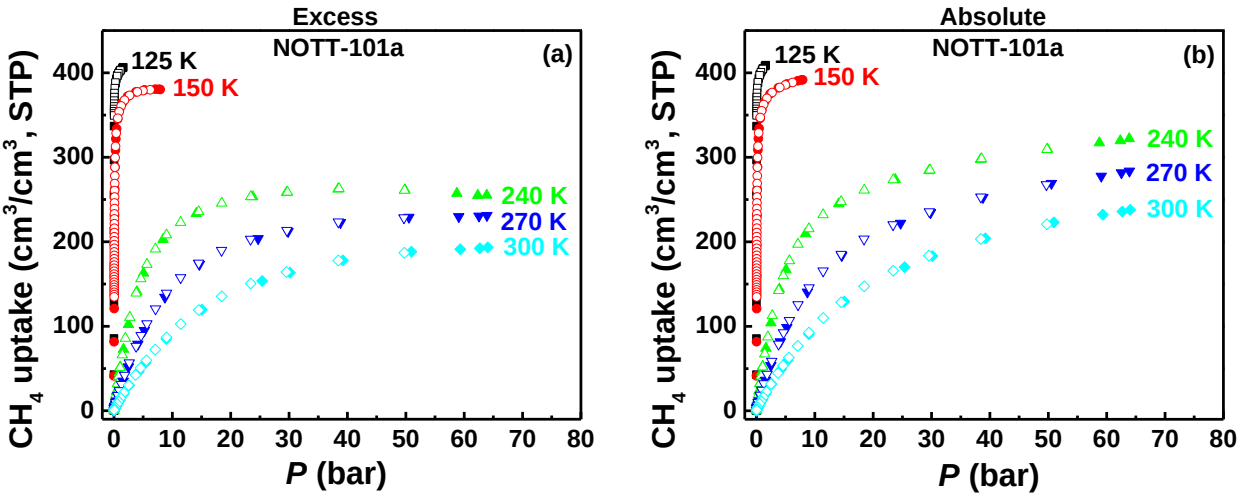

Figure S2. Excess (a) and absolute (b) high-pressure methane sorption isotherms of **NOTT-101a** at different temperatures. The filled and open symbols represent adsorption and desorption, respectively.

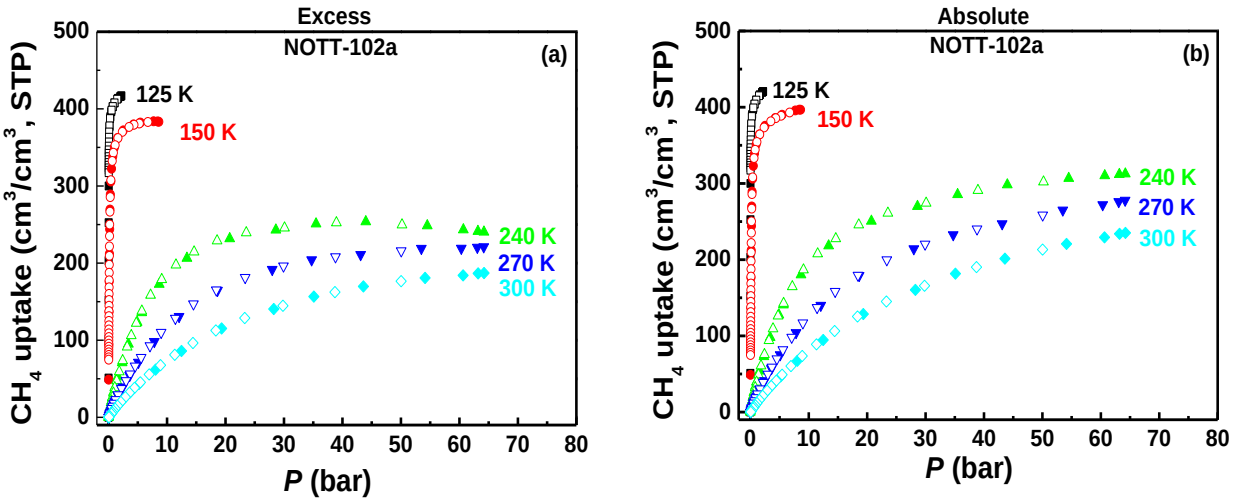

Figure S3. Excess (a) and absolute (b) high-pressure methane sorption isotherms of **NOTT-102a** at different temperatures. The filled and open symbols represent adsorption and desorption, respectively.

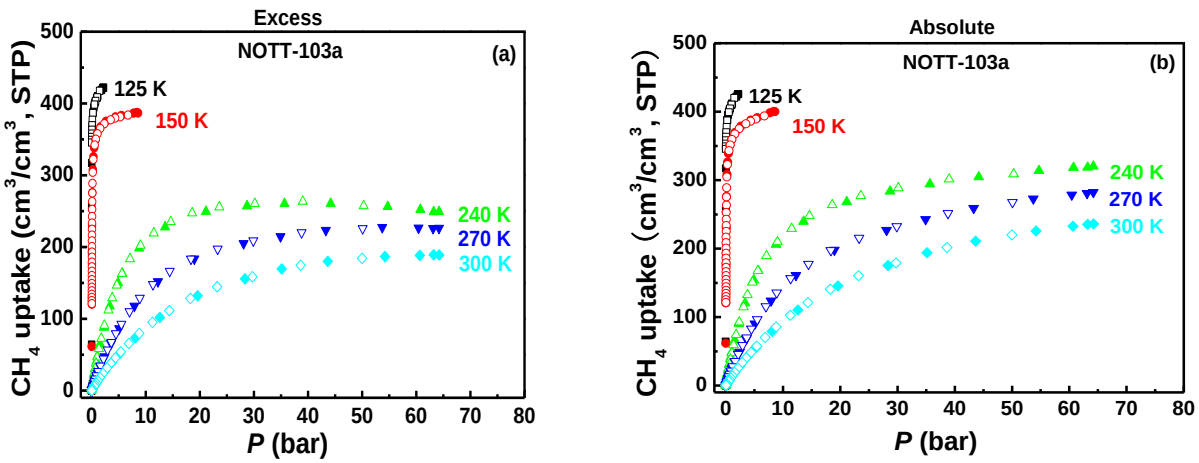

Figure S4. Excess (a) and absolute (b) high-pressure methane sorption isotherms of **NOTT-103a** at different temperatures. The filled and open symbols represent adsorption and desorption, respectively.

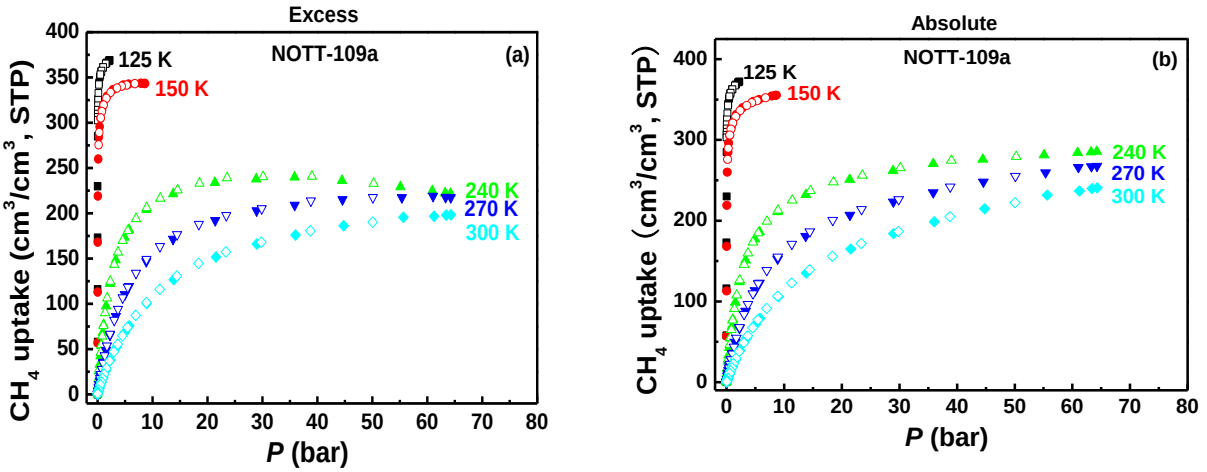

Figure S5. Excess (a) and absolute (b) high-pressure methane sorption isotherms of **NOTT-109a** at different temperatures. The filled and open symbols represent adsorption and desorption, respectively.

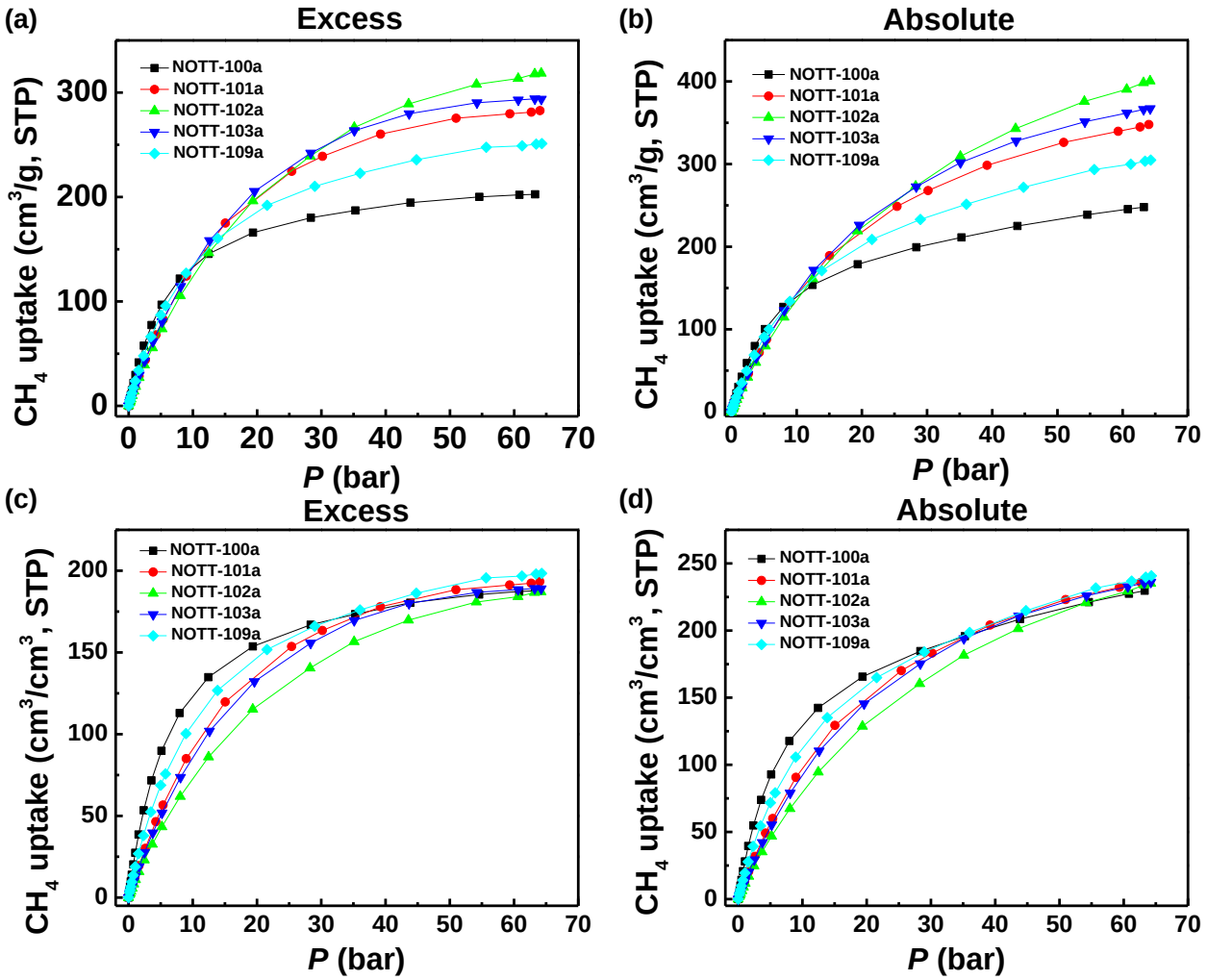

Figure S6. Excess (a) and absolute (b) gravimetric methane sorption isotherms at 300 K for all MOFs investigated. Excess (c) and absolute (d) volumetric methane sorption isotherms at 300 K for all MOFs investigated.

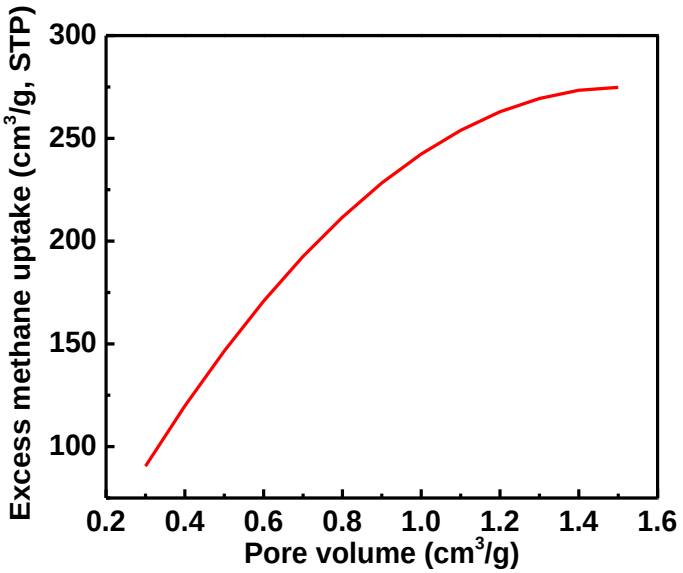

Figure S7. Excess methane uptake, C, (cm^3/g, STP) at 35 bar and 300 K *versus* pore volume, V_p, (cm^3/g) according to the empirical equation: $C = -126.69 \times V_p^2 + 381.62 \times V_p - 12.57$.

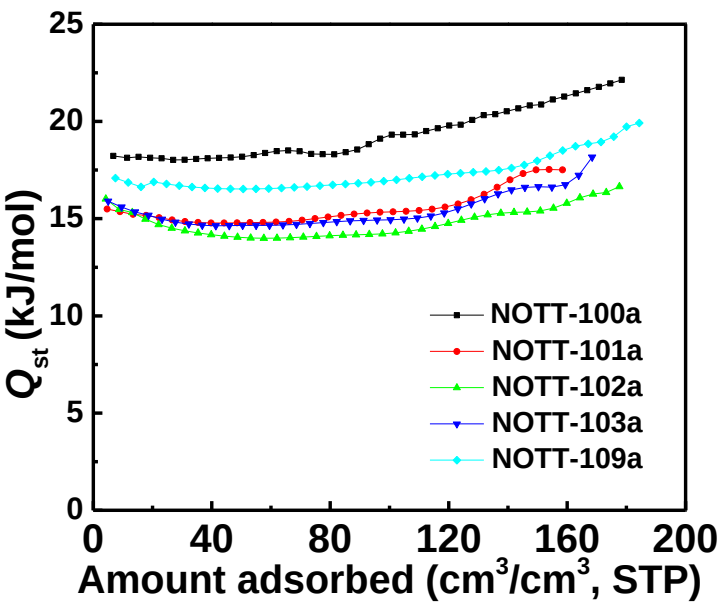

Figure S8. The loading dependence of the isosteric heat of methane adsorption in all MOF samples investigated.

Table S1. Methane adsorption in the selected MOFs.

MOFs	S_{BET}[a] [m²/g]	S_{BET}[a] [m²/cm³]	V_p[b] [cm³/g]	V_p[b] [cm³/cm³]	D_c[c] [g/cm³]	Excess CH_4 Uptake[d] [cm³/g] ([cm³/cm³])	Absolute CH_4 Uptake[d] [cm³/g] ([cm³/cm³])	Deliverable Capacity[e] [cm³/g] ([cm³/cm³])	d[f]	*Pore occupancy*[g]	*Reference*
NOTT-100a	1661	1539	0.677	0.627	0.9265	187 (173)	210 (195)	112 (104)	0.222	0.5466	This work
NOTT-109a	2110	1667	0.850	0.671	0.7899	222 (175)	248 (196)	158 (125)	0.208	0.5092	This work
NOTT-101a	2805	1918	1.080	0.739	0.6838	250 (171)	284 (194)	202 (***138***)	0.188	0.4493	This work
NOTT-103a	2958	1903	1.157	0.744	0.6432	263 (169)	300 (193)	218 (***140***)	0.185	0.4361	This work
NOTT-102a	3342	1962	1.268	0.745	0.5872	266 (156)	308 (181)	232 (**136**)	0.173	0.4064	This work
				--							
NiMOF-74a	1027	1239	0.44	0.531	1.2060	158 (190)	166 (200)	70 (84)	0.269		1
UTSA-40a	1630	1348	0.650	0.538	0.827	162 (134)	189 (156)	125 (103)	0.208		2
UTSA-20a	1655	1505	0.630	0.573	0.9096	196 (178)	214 (195)	111 (101)	0.242		3
PCN-14a	1753	1453	0.87	0.721	0.8288	252 (220)	264 (230)	157 (***137***)	0.217		4
NOTT-107a	1770	1338	0.767	0.580	0.7559	228 (172)	259 (196)	146 (110)	0.241		5
PCN-11a	1931	1445	0.91	0.681	0.7485	228 (171)	255 (191)	167 (125)	0.200		6
Cu-TDPAT-a	1938	1518	0.930	0.728	0.7832	200 (157)	231 (181)	135 (106)	0.177		7
SNU-50'a	2300	1495	0.9915	0.644	0.6499	265 (172)	306 (199)	204 (133)	0.220		8
SDU-8a	2516	1607	1.02	0.651	0.6386	196 (125)	230 (147)	155 (99)	0.161		9
SDU-7a	2713	1644	1.10	0.667	0.6060	226 (137)	264 (160)	185 (112)	0.171		9
SDU-6a	2826	1727	1.17	0.715	0.6112	242 (148)	282 (172)	203 (124)	0.172		9
ZJU-35a	2899	1906	1.156	0.760	0.6574	231 (152)	269 (177)	201 (132)	0.166		10
ZJU-25a	2998	1865	1.183	0.736	0.6220	249 (155)	288 (180)	211 (131)	0.174		11
PCN-61a	3000	1680	1.36	0.762	0.5600	259 (145)	307 (172)	227 (127)	0.161		12
NU-125a	3120	1803	1.29	0.746	0.578	272 (157)	316 (183)	226 (130)	0.175		13
PCN-66a	4000	1800	1.63	0.734	0.4500	244 (110)	302 (136)	224 (101)	0.132		12
ZJU-36a	4014	1990	1.599	0.793	0.4958	234 (116)	285 (141)	228 (113)	0.127		10
FJI-1a	4043	1637	1.430	0.579	0.4050	226 (91)	263 (107)	196 (79)	0.131		14
NOTT-119a	4118	1486	2.35	0.848	0.3608	216 (78)	301 (109)	243 (88)	0.091		15
NU-111a	4930	2016	2.09	0.855	0.409	266 (109)	337 (138)	266 (109)	0.115		16
PCN-68a	5109	1941	2.13	0.809	0.3800	260 (99)	337 (128)	258 (98)	0.113		12
DUT-49a	5476	1691	2.91	0.899	0.3088	266 (82)	368 (114)	162 (50)	0.090		17

[a] BET surface area; [b] pore volume; [c] framework density; [d] at 35 bar and room temperature; [e] Defined as the difference in adsorbed amount between 35 and 5 bar at room temperature; [f] Density of adsorbed methane in micropores; [g] pore occupancy under 35 bar and room temperature is defined as excess methane storage amount under 35 bar and room temperature divided by excess saturated methane storage amount, which was determined at 150 K. The absolute methane uptakes over 180 cm^3/cm^3 are highlighted in red. The delivery amounts of methane over 135 cm^3/cm^3 are highlighted in italic and bold.

Table S2: Comparison of the experimental excess methane uptakes at 35 bar and ambient temperature and the predicted ones according to the established empirical equation and pore volumes.[a,b]

MOFs	Experimental		Predicted	Reference
	Pore volume [cm^3/g]	Excess methane uptake at 35 bar [cm^3/g] ([cm^3/cm^3])	Excess methane uptake at 35 bar [cm^3/g] ([cm^3/cm^3])	
MOF-505a	0.677	187 (173)	188 (174)	This work
NOTT-109a	0.850	222 (175)	220 (174)	This work
NOTT-101a	1.080	250 (171)	251 (172)	This work
NOTT-103a	1.157	263 (169)	259 (167)	This work
NOTT-102a	1.268	266 (156)	267 (157)	This work
ZnMOF-74a	0.41	139 (171)	123 (151)	1
NiMOF-74a	0.44	158 (190)	131 (158)	1
CoMOF-74a	0.48	149 (174)	142 (165)	1
MnMOF-74a	0.50	146 (158)	147 (159)	1
UTSA-34b-a	0.542	168 (141)[a]	157 (132)	18
MIL-53(Cr)-a	0.56	159 (165)	161 (167)	19
$Cu(SiF_6)(4,4'\text{-bpy})_2$-a	0.56	146 (125)	161 (138)	20
MgMOF-74a	0.61	164 (149)	173 (157)	1
UTSA-20a	0.63	196 (178)	178 (162)	3
UTSA-40a	0.650	162 (134)	181 (150)	2
$Zn_2(bdc)_2(ted)$-a	0.68	167 (137)	188 (154)	21
HKUST-1a	0.76	200 (176)	204 (180)	22
NOTT-107a	0.767	226 (171)	206 (155)	5
PCN-14a	0.87	252 (220)[b]	224 (195)	4
PCN-11a	0.91	228 (171)	229 (172)	6
Cu-TDPAT-a	0.930	202 (158)	232 (182)	7
IRMOF-6a	0.944	240 (155)	234 (152)	23
SNU-50'a	0.9915	265 (172)	241 (157)	8
PCN-46a	1.012	243 (150)	244 (151)	24
SDU-8a	1.02	196 (125)	245 (156)	9
IRMOF-1a	1.04	227 (135)	247 (146)	23
PCN-16a	1.06	227 (164)	249 (181)	25
SDU-7a	1.10	226 (137)	254 (154)	9
$[Zn_3(OH)]_4(tbcppm)(H_2tbcppm)_2$-a	1.14	245 (166)	257 (174)	26
SDU-6a	1.17	242 (148)	260 (159)	9
ZJU-25a	1.183	249 (155)	261 (163)	11
NU-125a	1.29	272 (157)	269 (155)	13
PCN-61a	1.36	259 (145)	272 (152)	12

[a] reported in 290 K; [b] reported in 290 K, and using the solvated framework density of 0.871 cm^3/g.

Details of GCMC simulation

To locate the CH_4 adsorption sites other than the open Cu ions, we performed grand canonical Monte Carlo (GCMC) simulations of methane adsorption in the five MOFs (with the open Cu sites preoccupied by methane) using classical force-field method.[27] In the simulation, both the CH_4 molecules and the frameworks were treated as rigid bodies. The standard universal force field was used to describe the methane-framework interaction and the methane-methane interaction. A $2\times2\times1$ MOF supercell was used as the simulation box. 2×10^7 steps were used for equilibration and additional 2×10^7 steps were used to calculate the ensemble average of CH_4 adsorption sites and thermodynamic properties. More technical details of our GCMC simulations can also be found in our previous work.[28] Simulations were performed at T = 200 K, 300 K, and at various pressures. The probability distribution of adsorbed CH_4 was generated from the simulation after the equilibrium stage, and representative results are shown in Figure S9 to S11 as examples. It is clear from the results that with increasing pressure, CH_4 molecules first get adsorbed at the channels interconnecting the two pores, then the surfaces of the empty pore get populated (note that the surface of the other pore is already preoccupied by methane molecules on the Cu site), and finally the central voids of the two pores get filled. In **NOTT-100a** and **NOTT-109a**, the locations of the adsorbed methane are relatively well-defined because of their small pores. In contrast, the adsorption in the large pore of **NOTT-101a**, **NOTT-102a**, and **NOTT-103a** is much more diffused due to weaker methane-framework interaction. Finally, we note that at RT, the CH_4 adsorption locations identified are essentially the same, while the gas populations on different sites become less distinctive than those at 200 K.[30,31]

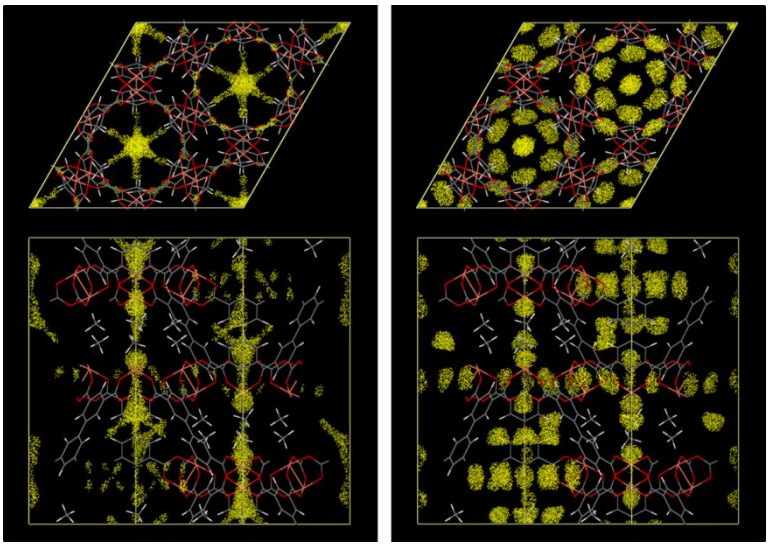

Figure S9. Probability distribution of the CH_4 center of mass in **NOTT-100a** (**MOF-505a)** unit cell (top view and side view), obtained from GCMC simulation at 200 K, and 0.001 bar (left) and 0.10 bar (right). The yellow regions represent the places where methane molecules are populated in the MOF structure. Note that the open-Cu site is preoccupied with CH_4 molecules in order to focus our effort on the search of other methane adsorption sites.

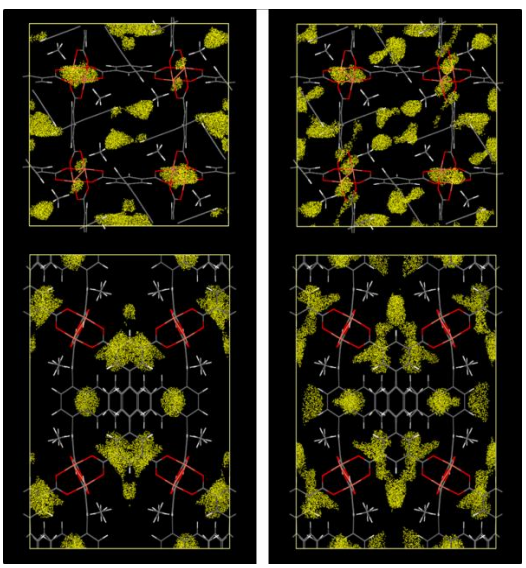

Figure S10. Probability distribution of the CH_4 center of mass in **NOTT-109a** unit cell (top view and side view), obtained from GCMC simulation at 200 K, and 0.001 bar (left) and 0.10 bar (right).

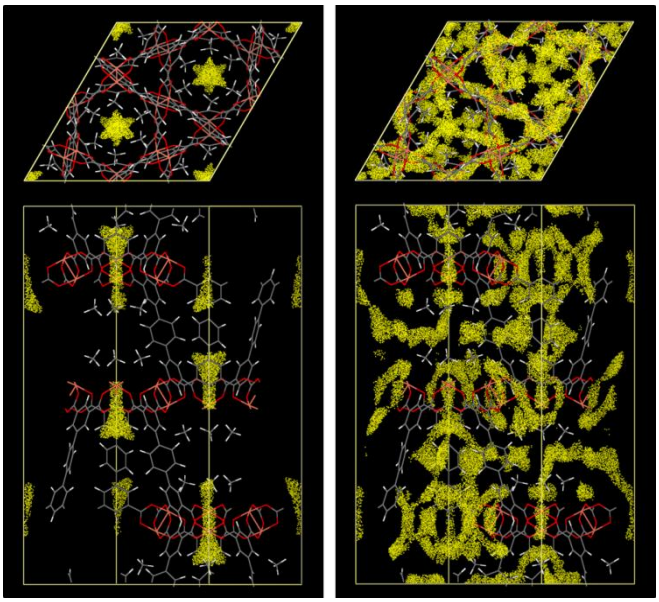

Figure S11. Probability distribution of the CH_4 center of mass in **NOTT-101a** unit cell (top view and side view), obtained from GCMC simulation at 200 K, and 0.001 bar (left) and 0.10 bar (right).

Disclaimer: Certain commercial equipment, instruments, or materials are identified in this paper to foster understanding. Such identification does not imply recommendation or endorsement by the National Institute of Standards and Technology, nor does it imply that the materials or equipment identified are necessarily the best available for the purpose.

References

(1) Wu, H.; Zhou, W.; Yildirim, T., High-Capacity Methane Storage in Metal-Organic Frameworks M_2(dhtp): The Important Role of Open Metal Sites. *J. Am. Chem. Soc.* **2009,** *131*, 4995-5000.

(2) He, Y.; Xiang, S.; Zhang, Z.; Xiong, S.; Wu, C.; Zhou, W.; Yildirim, T.; Krishna, R.; Chen, B., A microporous metal-organic framework assembled from an aromatic tetracarboxylate for H_2 purification. *J. Mater. Chem. A* **2013**, DOI: 10.1039/c2ta01260j.

(3) Guo, Z.; Wu, H.; Srinivas, G.; Zhou, Y.; Xiang, S.; Chen, Z.; Yang, Y.; Zhou, W.; O'Keeffe, M.; Chen, B., A Metal-Organic Framework with Optimized Open Metal Sites and Pore Spaces for High Methane Storage at Room Temperature. *Angew. Chem. Int. Ed.* **2011**, *50*, 3178-3181.

(4) Ma, S.; Sun, D.; Simmons, J. M.; Collier, C. D.; Yuan, D.; Zhou, H.-C., Metal-Organic Framework from an Anthracene Derivative Containing Nanoscopic Cages Exhibiting High Methane Uptake. *J. Am. Chem. Soc.* **2008**, *130*, 1012-1016.

(5) Wilmer, C. E.; Leaf, M.; Lee, C. Y.; Farha, O. K.; Hauser, B. G.; Hupp, J. T.; Snurr, R. Q., Large-scale screening of hypothetical metal-organic frameworks. *Nature Chem.* **2012,** *4*, 83-89.

(6) Wang, X.-S.; Ma, S.; Rauch, K.; Simmons, J. M.; Yuan, D.; Wang, X.; Yildirim, T.; Cole, W. C.; López, J. J.; Meijere, A. d.; Zhou, H.-C., Metal-Organic Frameworks Based on Double-Bond-Coupled Di-Isophthalate Linkers with High Hydrogen and Methane Uptakes. *Chem. Mater.* **2008,** *20*, 3145-3152.

(7) Li, B.; Zhang, Z.; Li, Y.; Yao, K.; Zhu, Y.; Deng, Z.; Yang, F.; Zhou, X.; Li, G.; Wu, H.; Nijem, N.; Chabal, Y. J.; Lai, Z.; Han, Y.; Shi, Z.; Feng, S.; Li, J., Enhanced Binding Affinity, Remarkable Selectivity, and High Capacity of CO_2 by Dual Functionalization of a rht-Type Metal-Organic Framework. *Angew. Chem. Int. Ed.* **2012**, *51*, 1412-1415.

(8) Prasad, T. K.; Hong, D. H.; Suh, M. P., High Gas Sorption and Metal-Ion Exchange of Microporous Metal-Organic Frameworks with Incorporated Imide Groups. *Chem. Eur. J.* **2010**, *16*, 14043-14050.

(9) Zhao, X.; Sun, D.; Yuan, S.; Feng, S.; Cao, R.; Yuan, D.; Wang, S.; Dou, J.; Sun, D., Comparison of the Effect of Functional Groups on Gas-Uptake Capacities by Fixing the Volumes of Cages A and B and Modifying the Inner Wall of Cage C in rht-Type MOFs. *Inorg. Chem.* **2012**, *51*, 10350-10355.

(10) Kong, G.-Q.; Han, Z.-D.; He, Y.; Ou, S.; Zhou, W.; Yildirim, T.; Krishna, R.; Zou, C.; O'Keeffe, M.; Wu, C.-D.; Chen, B., Porous metal-organic frameworks constructed from expanded organic building units with significant potential for use as adsorbents in hydrogen purification processes operating at high pressures. Submitted.

(11) Duan, X.; Yu, J.; Cai, J.; He, Y.; Wu, C.; Zhou, W.; Yildirim, T.; Zhang, Z.; Xiang, S.; O'Keeffe, M.; Chen, B.; Qian, G., A Microporous Metal-Organic Framework of a Rare sty-a Topology for High CH_4 Storage at Room Temperature. *Chem. Commun.* **2013,** *49*, 2043-2045.

(12) Yuan, D.; Zhao, D.; Sun, D.; Zhou, H.-C., An Isoreticular Series of Metal-Organic Frameworks with Dendritic Hexacarboxylate Ligands and Exceptionally High Gas-Uptake Capacity. *Angew. Chem. Int. Ed.* **2010,** *49*, 5357-5361.

(13) Wilmer, C. E.; Farha, O. K.; Yildirim, T.; Eryazici, I.; Krungleviciute, V.; Sarjeant, A. A.; Snurr, R. Q.; Hupp, J. T., Gram-scale, high-yield synthesis of a robust metal-organic framework for storing methane and other gases. *Energy Environ. Sci.* **2013**, *6*, 1158-1163.

(14) Han, D.; Jiang, F.-L.; Wu, M.-Y.; Chen, L.; Chen, Q.-H.; Hong, M.-C., A non-interpenetrated porous metal-organic framework with high gas-uptake capacity. *Chem. Commun.* **2011**, *47*, 9861-9863.

(15) Yan, Y.; Yang, S.; Blake, A. J.; Lewis, W.; Poirier, E.; Barnett, S. A.; Champness, N. R.; Schröder, M., A mesoporous metal-organic framework constructed from a nanosized C_3-symmetric linker and [Cu_{24}(isophthalate)$_{24}$] cuboctahedra. *Chem. Commun.* **2011**, *47*, 9995-9997.

(16) Peng, Y.; Srinivas, G.; Wilmer, C. E.; Snurr, R. Q.; Hupp, J. T.; Yildirim, T.; Farha, O. K., Simultaneously High Gravimetric and Volumetric Gas Uptake Characteristics of the Metal-Organic Framework NU-111. *Chem. Commun.* **2013**, *49*, 2992-2994.

(17) Stoeck, U.; Krause, S.; Bon, V.; Senkovska, I.; Kaskel, S., A highly porous metal-organic framework, constructed from a cuboctahedral super-molecular building block, with exceptionally high methane uptake. *Chem. Commun.* **2012**, *48*, 10841-10843.

(18) Y. He, Z. Zhang, S. Xiang, H. Wu, F. R. Fronczek, W. Zhou, R. Krishna, M. O'Keeffe and B. Chen, *Chem. Eur. J.*, **2012**, *18*, 1901-1904.

(19) Bourrelly, S.; Llewellyn, P. L.; Serre, C.; Millange, F.; Loiseau, T.; Férey, G., Different Adsorption Behaviors of Methane and Carbon Dioxide in the Isotypic Nanoporous Metal Terephthalates MIL-53 and MIL-47. *J. Am. Chem. Soc.* **2005**, *127*, 13519-13521.

(20) Noro, S.-i.; Kitagawa, S.; Kondo, M.; Seki, K., A New, Methane Adsorbent, Porous Coordination Polymer [{$CuSiF_6$(4,4'-bipyridine)$_2$}$_n$]. *Angew. Chem. Int. Ed.* **2000**, *39*, 2082-2084.

(21) Kim, H.; Samsonenko, D. G.; Das, S.; Kim, G.-H.; Lee, H.-S.; Dybtsev, D. N.; Berdonosova, E. A.; Kim, K., Methane Sorption and Structural Characterization of the Sorption Sites in Zn_2(bdc)$_2$(dabco) by Single Crystal X-ray Crystallography. *Chem. Asian J.* **2009**, *4*, 886-891.

(22) Senkovska, I.; Kaskel, S., High pressure methane adsorption in the metal-organic frameworks Cu_3(btc)$_2$, Zn_2(bdc)$_2$dabco, and $Cr_3F(H_2O)_2O$(bdc)$_3$. *Microporous Mesoporous Mater.* **2008**, *112*, 108-115.

(23) Eddaoudi, M.; Kim, J.; Rosi, N.; Vodak, D.; Wachter, J.; O'Keeffe, M.; Yaghi, O. M., Systematic Design of Pore Size and Functionality in Isoreticular MOFs and Their Application in Methane Storage. *Science* **2002,** *295*, 469-472.

(24) Zhao, D.; Yuan, D.; Yakovenko, A.; Zhou, H.-C., A NbO-type metal-organic framework derived from a polyyne-coupling di-isophthalate linker formed in situ. *Chem. Commun.* **2010**, *46*, 4196-4198.

(25) Sun, D.; Ma, S.; Simmons, J. M.; Li, J.-R.; Yuan, D.; Zhou, H.-C., An unusual case of symmetry-preserving isomerism. *Chem. Commun.* **2010**, *46*, 1329-1331.

(26) Liu, D.; Wu, H.; Wang, S.; Xie, Z.; Li, J.; Lin, W., A high connectivity metal-organic framework with exceptional hydrogen and methane uptake capacities. *Chem. Sci.* **2012**, *3*, 3032-3037.

(27) D. Frenkel and B.Smit, *Understanding Molecular Simulation: From Algorithms to Applications.* San Diego: Academic Press, 2002.

(28) Wu, H.; Simmons, J. M.; Liu, Y.; Brown, C. M.; Wang, X.-S.; Ma, S.; Peterson, V. K.; Southon, P. D.; Kepert, C. J.; Zhou, H.-C.; Yildirim, T.; Zhou, W., Metal-Organic Frameworks with Exceptionally High Methane Uptake: Where and How is Methane Store. *Chem. Eur. J.* **2010**, *16*, 5205-5214.

(29) Bhattacharya, S.; Gubbins, K. E., Fast Method for Computing Pore Size Distributions of Model Materials. *Langmuir* **2006**, *22*, 7726-7731.

(30) Karra, J. R.; Walton, K. S., Effect of Open Metal Sites on Adsorption of Polar and Nonpolar Molecules in Metal-Organic Framework Cu-BTC. *Langmuir* **2008**, *24*, 8620-8626.

(31) Lucena, S. M. P.; Mileo, P. G. M.; Silvino, P. F. G.; Cávio L. Cavalcante, J., Unusual Adsorption Site Behavior in PCN-14 Metal-Organic Framework Predicted from Monte Carlo Simulation. *J. Am. Chem. Soc.* **2011**, *133*, 19282-19285.